Electroactive Self-Assembled Biferrocenyl Alkanethiol Monolayers on Au(111) Surface and on Gold Nanoclusters

Teng-Yuan Dong,* Ling-Shao Chang, I-Min Tseng, and Shu-Jen Huang

Department of Chemistry, Center for Nanoscience and Nanotechnology, National Sun Yat-Sen University, Kaohsiung, Taiwan

Received October 6, 2003. In Final Form: January 2, 2004

The spectroscopic and electrochemical characterizations of electrochemically stable biferrocene-modified Au clusters and chemisorbed biferrocenylalkanethiols on Au(111) surface were studied. The characterizations of biferrocene-modified Au cluster using TEM, UV−vis, and NMR techniques are also reported. Two successive reversible one-electron redox waves were observed for the biferrocenylalkanethiol Au nanoclusters and biferrocenylalkanethiol monolayers on Au(111) surface in the cyclic voltammetry. Furthermore, the positive and negative current peaks for each redox wave occur at almost the same potential, and the peak current increases almost linearly with the sweep rate. Repeat scanning does not change the voltammograms, demonstrating that these monolayers are stable to electrochemical cycling. The coverages of electroactive biferrocene in the monolayers were calculated from the cyclic voltammograms. The standard electron-transfer rate constant was calculated from the splitting between the oxidation and reduction peaks.

Introduction

This paper describes a synthetic pathway to, and the spectroscopic and electrochemical characterizations of, stable biferrocenyl alkanethiolate monolayer-protected Au clusters (MPCs) and biferrocenyl alkanethiolate self-assembled monolayers (SAMs) on Au(111) surface. Our work builds on the growing body of knowledge of self-assembly technique monolayers.

The literatures of alkanethiolate Au-based monolayers include examples of ferrocenyl alkanethiols ($Fc(CH_2)_nSH$, $Fc = (C_5H_5)Fe(C_5H_4)$),[1−5] carbonyl-functionalized ferrocenoyl alkanethiols ($FcCO(CH_2)_nSH$) and $FcCO_2(CH_2)_nSH$),[4−12] and carbonyl-functionalized biferrocenoyl alkanethiols ($BifcCO(CH_2)_nSH$, $Bifc = (C_5H_5)Fe(C_{10}H_{10})Fe(C_5H_5)$),[13−15] but none that are biferrocenylalkanethiols ($Bifc(CH_2)_nSH$). The pioneered studies of electroactive self-assembled monolayers (SAMs) of ferrocene-terminated alkanethiols coadsorption with unsubstituted *n*-alkanethiols on evaporated gold films were reported by Chidsey.[4,16] Monolayers containing low concentrations (mole fraction (χ_{Fc}) ≤ 0.25) of alkanethiols linked to ferrocene by a polar ester group ($FcCO_2(CH_2)_n$-SH) coadsorption with $CH_3(CH_2)_nSH$, ($n = 7, 9, 11$) show thermodynamically ideal surface electrochemistry. At low mole fraction, the oxidation and reduction peaks are symmetric and with no splitting between the oxidation and reduction peaks. The lack of peak splitting indicates that the rate of electron transfer is rapid on the time scale of the electrochemical experiment. Chidsey suggested that the ferrocene groups to be homogeneous and noninteracting. At higher mole fractions of the electroactive thiol in the adsorption solution, the resulting cyclic voltammograms broaden, develop an asymmetry, and finally develop an additional set of peaks as the amount of ferrocene is increased. Chidsey suggested that the breakdown of the thermodynamically ideal behavior of this system is probably due to a combination of interaction between ferrocene sites and inhomogeneity of those sites at higher surface contractions. Use of ferrocene-terminated thiols ($Fc(CH_2)_{11}SH$) in which the ferrocene is attached directly to the polymethylene chain without a polar ester group leads to broadened electrochemical features, even at the lowest fraction ($\chi_{Fc} = 0.05$) examined. This highly nonideal behavior at low surface coverage suggests a strong interaction between the ferrocene groups, perhaps due to aggregation.

It has been reported that the ferrocenoyl alkanethiol SAMs can be complexed effectively by the sparingly water-soluble, amphiphilic calixarene host.[7]

Following the report by Brust et al. on the synthesis of gold clusters stabilized by monolayers of alkanethiolate ligands,[17,18] Murray et al. launched an investigation of their synthesis as to the core size and their chemical, electrochemical, structural, and physical properties in ferrocenyl alkanethiolate Au clusters.[8−12] The voltam-

(1) Collard, D. M.; Fox, M. A. *Langmuir* **1991**, *7*, 1192−1197.
(2) Uosaki, K.; Sato, Y.; Kita, H. *Langmuir* **1991**, *7*, 1510−1514.
(3) Ingram, R. S.; Hostetlar, M. J.; Murray, R. W. *J. Am. Chem. Soc.* **1997**, *119*, 9175−9178.
(4) Chidsey, C. E. D.; Bertozzi, C. R.; Putvinski, T. M.; Mujsce, A. M. *J. Am. Chem. Soc.* **1990**, *112*, 4301−4306.
(5) (a) Ingram, R. S.; Hostetler, M. J.; Murray, R. W.; Schaaf, T. G.; Khoury, J. T.; Whetten, R. L.; Bigioni, T. P.; Guthrie, D. K.; First, P. N. *J. Am. Chem. Soc.* **1997**, *119*, 9279−9280. (b) Chen, S.; Ingram, R. S.; Hostetler, M. J.; Pietron, J. J.; Murray, R. W.; Schaaff, T. G.; Khoury, J. T.; Alvarez, M. M.; Whetten, R. L. *Science* **1998**, *280*, 2098−2101.
(6) Viana, A. S.; Abrantes, L. M.; Jin, G.; Floate, S.; Nichols, R. J.; Kalaji, M. *Phys. Chem. Chem. Phys.* **2001**, *3*, 3411−3419.
(7) Zhang, L.; Godinez, L. A.; Lu, T.; Gokel, G. W.; Kaifer, A. E. *Angew. Chem., Int. Ed. Engl.* **1995**, *34*, 235−237.
(8) Green, S. J.; Stokes, J. J.; Hostetler, M. J.; Pietron, J. J.; Murray, R. W. *J. Phys. Chem. B* **1997**, *101*, 2663−2668.
(9) Terrill, R. H.; Postlethwaite, T. A.; Chen, C.-H.; Poon, C.-D.; Terzis, A.; Chen, A.; Hutchison, J. E.; Clark, M. R.; Wignall, G.; Londono, J. D.; Superfine, R.; Falvo, M.; Johnson, C. S.; Samulski, E. T.; Murray, R. W. *J. Am. Chem. Soc.* **1995**, *117*, 12537−12548.
(10) Hostetler, M. J.; Green, S. J.; Stokes, J. J.; Murray, R. W. *J. Am. Chem. Soc.* **1996**, *118*, 4212−4213.
(11) Hostetler, M. J.; Wingate, J.; Zhong, C.-J.; Harris, J. E.; Vachet, R. W.; Clark, M. R.; Londono, J. D.; Green, S. J.; Stokes, J. J.; Wignall, G. W.; Glish, G. L.; Porter, M. D.; Evans, N. D.; Murray, R. W. *Langmuir* **1998**, *14*, 17−30.
(12) Green, S. J.; Pietron, J. J.; Stokes, J. J.; Hostetler, M. J.; Vu, H.; Wuelfing, W. P.; Murray, R. W. *Langmuir* **1998**, *14*, 5612−5619.
(13) Kubo, K.; Kondow, H.; Nishihara, H. *Electrochemistry* **1999**, *12*, 1129−1131.
(14) Horikoshi, T.; Itoh, M.; Kurihara, M.; Kubo, K.; Nishihara, H. *J. Electroanal. Chem.* **1999**, *473*, 113−116.
(15) Men, Y.; Kubo, K.; Kurihara, M.; Nishihara, H. *Phys. Chem. Chem. Phys.* **2001**, *3*, 3427−3430.
(16) Chidsey, C. E. D. *Science* **1991**, *251*, 919−922.

10.1021/la0303714 CCC: $27.50
Published on Web 04/27/2004

Scheme 1

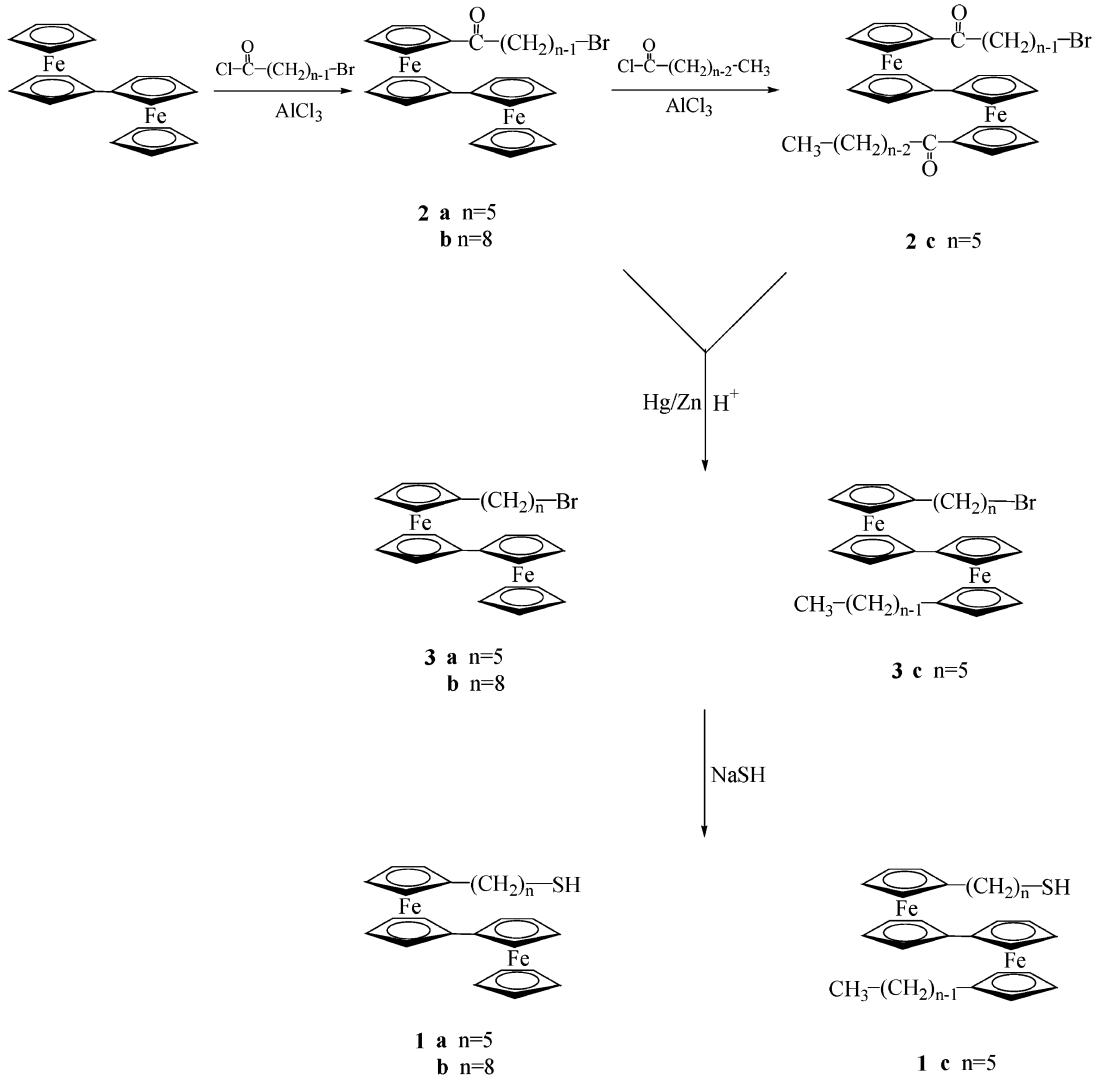

metric results show that ferrocenyl alkanethiolate Au clusters not only exhibit ferrocene electrochemistry but also exhibit a double layer charging phenomenon analogous to that of a metal electrode/solution interface. The CV results reveal physisorption of clusters acted as tiny electrodes on the working electrode.

Biferrocene takes a two-step one-electron redox process with the formation of the mixed-valence state. Nishihara reported[13−15] the electrochemical properties of the SAMs of Bifc$CO(CH_2)_n$SH on Au electrode and of Bifc$CO(CH_2)_n$-SH-modified Au clusters. The Bifc$CO(CH_2)_n$SH-modified Au cluster undergoes a two-step one-electron redox process in CH_2Cl_2 solution. However, the shape of the voltammogram changes gradually during the potential scans, and it converts finally into one broad redox wave. Our strategy is the use of redox stable biferrocenyl alkanethiols (Bifc$(CH_2)_n$SH, n = 5 for **1a**, n = 8 for **1b**, and (C_5H_{11})Bifc$(CH_2)_5$SH (**1c**)) in which the biferrocene is attached directly to the polymethylene chain without a polar carbonyl group. We report the electrochemical properties of the SAMs of **1** on Au(111) surface and the characterizations and electrochemical properties of the Au MPCs of **1**.

(17) Brust, M.; Walker, M.; Bethell, D.; Schiffrin, D. J.; Whyman, R. *J. Chem. Soc., Chem. Commun.* **1994**, 801−802.

(18) Brust, M.; Fink, J.; Bethell, D.; Schiffrin, D. J.; Kiely, C. J. *J. Chem. Soc., Chem. Commun.* **1995**, 1655−1656.

Experimental Section

Chemicals. The preparations involving air-sensitive materials were carried out by using standard Schlenk techniques under an atmosphere of N_2 (Scheme 1). Chromatography was performed on neutral Al_2O_3 (act. II). Dried CH_2Cl_2 was distilled from P_2O_5. The sample of biferrocene (Bifc) was prepared according to the literature procedure.[19]

The biferrocene derivatives (**1a**−**c**) were prepared from biferrocene. The acylating reagent was made up according to the Friedel−Crafts synthesis by mixing acyl chloride and excess $AlCl_3$ in dried CH_2Cl_2 for 20 min at 0 °C under N_2. The excess of $AlCl_3$ was filtered out with glass wool. The acylating reagent was added by means of a dropping funnel over a period of ∼1 h to a solution of biferrocene in dried CH_2Cl_2 at −78 °C. The reaction mixture was stirred for 6 h at −78 °C. The resulting mixture was separated after the reduction of ferrocenium ion with aqueous $Na_2S_2O_3$. The organic layer was washed with saturated aqueous $NaHCO_3$ and water, and it was then dried over $MgSO_4$. The solvent was removed under reduced pressure. The red residue was chromatographied. For **2a** and **2b**, elution with CH_2Cl_2/hexane (1:1) gave the staring material, and continued elution with CH_2Cl_2 gave the desired compounds. In the case of **2c**, elution with CH_2Cl_2 gave the starting material, and continued elution with CH_2Cl_2/EA (5:1) gave the desired compound. The physical properties of **2a** are as follows: ^{1}H NMR (500 MHz, $CDCl_3$): δ1.70 (m, 2H, $-CH_2-$), 1.87 (m, 2H, $-CH_2-$), 2.44 (t, 2H, $-CH_2-$), 3.42 (t, 2H, $-CH_2-$), 3.98 (s, 5H, Cp), 4.22 (dd, 4H, Cp), 4.33 (dd,

(19) Neuse, E. W. *J. Macromol. Sci. Chem. A* **1981**, *16*, 3−72.

4H, Cp), 4.36 (dd, 4H, Cp), 4.59 (dd, 2H, Cp); mp 80.0−80.5 °C. Mass spectrum (EI): M^+ at *m/z* 532, 534. Anal. calcd. for $C_{25}H_{25}BrFe_2O$: C, 56.29, H, 4.69. Anal. found: C, 56.28, H, 4.85. The physical properties of **2b** are as follows: ^{1}H NMR (500 MHz, $CDCl_3$): δ1.33 (m, 4H), 1.42 (m, 2H), 1.57 (m, 2H), 1.87 (m, 2H), 2.44 (t, 2H), 3.42 (t, 2H), 3.97 (s, 5H, Cp), 4.20 (m, 4H, Cp), 4.31 (dd, 2H, Cp), 4.35 (m, 4H, Cp), 4.58 (dd, 2H, Cp); mp 87.0−88.0 °C. Mass spectrum (EI): M^+ at *m/z* 574, 576. Anal. calcd. for $C_{28}H_{31}BrFe_2O$: C, 58.47, H, 5.43. Anal. found: C, 58.53, H, 5.53. The physical properties of **2c** are as follows: ^{1}H NMR (500 MHz, $CDCl_3$): δ0.93 (t, 3H, $-CH_3$), 1.33 (m, 2H, $-CH_2-$), 1.57 (m, 2H, $-CH_2-$), 1.71 (m, 2H, $-CH_2-$), 1.87 (m, 2H, $-CH_2-$), 2.44 (t, 4H, $-CH_2-$), 3.42 (t, 2H, $-CH_2-$), 4.26 (m, 4H, Cp), 4.30 (dd, 2H, Cp), 4.32 (dd, 2H, Cp), 4.35 (m, 4H, Cp), 4.57 (m, 4H, Cp); mp 104.0−105.0 °C. Mass spectrum (EI): M^+ at *m/z* 616, 618. Anal. calcd. for $C_{30}H_{33}BrFe_2O_2$: C, 58.39, H, 5.39. Anal. found: C, 58.08, H, 5.54.

The reduction reaction of **2** was carried out by adding Zn/Hg to a mixture solution (5 mL of toluene, 6 mL of water and 13.0 mL of concentrated HCl) of **2** (3.24 mmol). The resulting solution was refluxed under N_2 for 48 h. The organic layer was washed with H_2O until neutral. The water layer was extracted with ether. The combined extracts were dried over $MgSO_4$. After the evaporation of the solvent, the crude product was chromatographed. Elution with hexane gave the desired compound. The physical properties of **3a** are as follows: ^{1}H NMR (500 MHz, $CDCl_3$): δ1.38 (m, 4H), 1.82 (m, 2H), 2.11 (t, 2H, $-CH_2-$), 3.38 (t, 2H, $-CH_2-$), 3.85 (dd, 2H, Cp), 3.89 (dd, 2H, Cp), 3.98 (s, 5H, Cp), 4.12 (dd, 2H, Cp), 4.18 (dd, 2H, Cp), 4.26 (dd, 2H, Cp), 4.35 (dd, 2H, Cp); mp 94.0−96.0 °C. Mass spectrum (EI): M^+ at *m/z* 518, 520. Anal. calcd. for $C_{25}H_{27}BrFe_2$: C, 58.84, H, 5.24. Anal. found: C, 57.83, H, 5.37. The physical properties of **3b** are as follows: ^{1}H NMR (500 MHz, $CDCl_3$): δ1.25 (m, 6H, $-CH_2-$), 1.37 (m, 2H, $-CH_2-$), 1.41 (m, 2H, $-CH_2-$), 2.10 (t, 2H, $-CH_2-$), 3.41 (t, 2H, $-CH_2-$), 3.84 (dd, 2H, Cp), 3.88 (dd, 2H, Cp), 3.98 (s, 5H, Cp), 4.12 (dd, 2H, Cp), 4.16 (dd, 2H, Cp), 4.25 (dd, 2H, Cp), 4.34 (dd, 2H, Cp); mp 99.0−100.0 °C. Mass spectrum (EI): M^+ at *m/z* 560, 562. Anal. calcd. for $C_{28}H_{33}BrFe_2$: C, 59.93, H, 5.93. Anal. found: C, 59.94, H, 5.94. The physical properties of **3c** are as follows: ^{1}H NMR (500 MHz, $CDCl_3$): δ0.87 (t, 3H, $-CH_3$), 1.26 (m, 4H, $-CH_2-$), 1.38 (m, 4H, $-CH_2-$), 1.81 (t, 4H, $-CH_2-$), 2.09 (t, 4H, $-CH_2-$), 3.38 (t, 2H, $-CH_2-$), 3.83 (s, 4H, Cp), 3.88 (dd, 4H, Cp), 4.12 (dd, 4H, Cp), 4.24 (dd, 4H, Cp); mp 34.0−36.0 °C. Mass spectrum (EI): M^+ at *m/z* 588, 590. Anal. calcd. for $C_{30}H_{37}BrFe_2$: C, 61.15, H, 6.33. Anal. found: C, 61.20, H, 6.51.

Compound **3** (0.17 mmol) was reacted with excess NaSH in dried THF (60 mL) at reflux for 2 h. After the reduction with $Na_2S_2O_{3(aq)}$, the organic layer was washed with H_2O, and then it was dried over $MgSO_4$. The solvent was removed under reduced pressure. The crude product was chromatographied with hexane as elution solvent. The physical properties of **1a** are as follows: ^{1}H NMR ($CDCl_3$, δ): 1.36 (m, 2H, $-CH_2-$), 1.42 (m, 2H, $-CH_2-$), 1.66 (m, 2H, $-CH_2-$), 2.14 (t, 2H, $-CH_2-$), 2.67 (t, 2H, $-CH_2-$), 3.85 (dd, 2H, Cp), 3.89 (dd, 2H, Cp), 4.01 (s, 5H, Cp), 4.12 (dd, 2H, Cp), 4.18 (dd, 2H, Cp), 4.26 (dd, 2H, Cp), 4.34 (dd, 2H, Cp); ^{13}C NMR ($CDCl_3$, δ): 28.41 (Cp−$(CH_2)_2$−**C**H_2−), 28.66 (Cp−**C**H_2−), 29.07 (Cp−$(CH_2)_3$−**C**H_2−), 30.57 (Cp−CH_2−**C**H_2−), 39.00 (Cp−$(CH_2)_4$−**C**H_2−), 66.15 (Cp), 66.59 (Cp), 67.61 (Cp), 68.09 (Cp), 68.19 (Cp), 69.15 (Cp), 83.60 (Cp), 83.97 (Cp), 89.41 (Cp); mp 62.0−63.0 °C. Mass spectrum (EI): M^+ at *m/z* 472. Anal. calcd. for $C_{25}H_{28}Fe_2S$: C, 63.58, H, 5.97. Anal. found: C, 63.99, H, 5.93. The physical properties of **1b** are as follows: ^{1}H NMR ($CDCl_3$, δ): 1.25 (m, 2H, $-CH_2-$), 1.26 (m, 2H, $-CH_2-$), 1.27 (m, 2H, $-CH_2-$), 1.35 (m, 2H, $-CH_2-$), 1.38 (m, 2H, $-CH_2-$), 1.68 (m, 2H, $-CH_2-$), 2.10 (t, 2H, $-CH_2-$), 2.68 (t, 2H, $-CH_2-$), 3.84 (dd, 2H, Cp), 3.88 (dd, 2H, Cp), 3.98 (s, 5H, Cp), 4.12 (dd, 2H, Cp), 4.17 (dd, 2H, Cp), 4.26 (dd, 2H, Cp), 4.34 (dd, 2H, Cp); ^{13}C NMR ($CDCl_3$, δ): 28.52 (Cp−$(CH_2)_5$−**C**H_2−), 28.83 (Cp−**C**H_2−), 29.19 (Cp−$(CH_2)_6$−**C**H_2−), 29.21 (Cp−$(CH_2)_4$−**C**H_2−), 29.35 (Cp−$(CH_2)_3$−**C**H_2−), 29.50 (Cp−$(CH_2)_2$−**C**H_2−), 30.98 (Cp−**C**H_2−**C**H_2−), 39.18 (Cp−$(CH_2)_7$−**C**H_2−), 66.17 (Cp), 66.61 (Cp), 68.10 (Cp), 68.17 (Cp), 69.15 (Cp), 69.20 (Cp), 83.69 (Cp), 83.90 (Cp), 89.92 (Cp); mp 43.0−44.0 °C. Mass spectrum (EI): M^+ at *m/z* 514. Anal. calcd. for $C_{28}H_{34}Fe_2S$: C, 65.38, H, 6.66. Anal. found: C, 65.12, H, 6.66. The physical properties of **1c** are as follows: ^{1}H NMR ($CDCl_3$, δ): 0.89 (t, 3H, $-CH_3$), 1.24 (m, 4H, $-CH_2-$), 1.30 (m, 2H, $-CH_2-$), 1.39 (m, 4H, $-CH_2-$), 1.64 (m, 2H, $-CH_2-$), 2.11 (t, 4H, $-CH_2-$), 2.65 (t, 2H, $-CH_2-$), 3.85 (s, 4H, Cp), 3.89 (dd, 2H, Cp), 3.92 (dd, 4H, Cp), 4.13 (dd, 4H, Cp), 4.25 (dd, 4H, Cp); ^{13}C NMR ($CDCl_3$, δ): 14.07(−**C**H_3), 22.51 (**C**H_2–CH_3), 28.74 (Cp−**C**H_2−), 28.74 (−**C**H_2−$(CH_2)_2$–SH), 29.05 (−**C**H_2–CH_2–SH), 30.67 (Cp−CH_2−**C**H_2−), 31.77 (−**C**H_2–CH_2–CH_3), 39.02 (−**C**H_2–SH), 66.45 (Cp), 68.05 (Cp), 69.17 (Cp), 69.65 (Cp), 83.54 (Cp), 83.76 (Cp), 89.41 (Cp), 89.87 (Cp); mp 34.0−36.0 °C. Mass spectrum (EI): M^+ at *m/z* 542.

Preparation of Au MPCs. Octanethiolate-stablized Au MPCs were prepared as described by Murray.[11] In short, toluene solutions containing a 2:1 mole ratio of octanethiol to $HAuCl_4$ were reduced at room temperature with $NaBH_4$. The Au MPCs have 2.2 ± 0.7 nm average core diameters (by transmission electron microscopy) and an average formula of $Au_{309}(C_8)_{92}$ (by elementary analysis). The ∼2 nm sized particles were used to induce size and shape evolution with heating treatment. The ∼2 nm sized particles were dissolved in small amount of toluene together with tetraoctylammonium bromide and octanethiol.[20] The solution was heated in a silicone oil bath at 138 °C. When the color of this solution changed form brown to dark red, the solution was followed by further heating at ∼110 °C for 5 h. This color change involved a size evolution. The solution was subjected to solvent removal in a rotary evaporator (at ∼50 °C) followed by multiple cleaning using ethanol and acetone. The Au MPCs (AuC_8) with heating treatment have ∼4.5 nm core diameters (by transmission electron microscopy).

Formation of the SAMs (4a−c). The SAMs was prepared using an Au(111) single-crystal electrode (1 cm diameter, MaTeck, Jülich, Germany) that was polish with 0.05 μm alumina followed by cleaning with water, CH_2Cl_2, and ethanol. The thiol monolayers were prepared by soaking Au(111) electrodes in ethanol solutions of a biferrocene-terminated thiol (**1a**−**c**) and unsubstituted thiol at 1 mM total thiol concentration. The mole fraction of biferrocene-terminated thiol in the solution to total thiol in the solution to total thiol is denoted χ_{Bifc} and is varied from 0.1 to 1.0. The samples were removed from the adsorption solution after 24 h and washed with ethanol several times.

Formation of the MPCs (5a−c). A mixture of 4.5 nm Au MPCs (53 mg) and **1** (10 mg) in 1 mL toluene was stirred at room temperature for 48 h. The solvent was removed under vacuum. The resulting product was suspended in acetone and isolated with centrifuge. This procedure was repeated several times to obtain purified MPCs.

Electrochemical Measurements. Cyclic voltammetry was performed using a BAS 100 W system. The reference electrode was Ag/AgCl in saturated KCl solution. The cell used for the SAMs was a modified "drop cell".[21] Figure 1 shows a schematic of the drop cell. The Au(111) electrode (1 cm diameter, 0.7854 cm^2 geometric area) was fully covered with a stable drop of 1M $HClO_{4(aq)}$ solution which allows the area examined without mechanical contact. The $HClO_4$ electrolyte solution was degassed for 10 min prior to the start of measurement. After the air in the glass chamber was exchanged with N_2, the Pt counter electrode, the electrolyte solution and a reference electrode were inserted into the chamber from above. In the cases of free biferrocenyl alkanethiols and MPCs, the CV measurements were carried out in a standard three-compartment cell under N_2 at 25 °C equipped with a Pt counter electrode, glassy carbon working electrode and Ag/AgCl reference electrode in CH_2Cl_2/CH_3CN (1:1) solution containing 0.1 M (n-$C_4H_9)_4NPF_6$ electrolyte. Under these conditions, ferrocene shows a reversible redox process at $E_{1/2}$ = 0.44 V.

Physical Methods. ^{1}H and ^{13}C NMR spectra were run on a Varian UNITY INOVA-500 spectroscopy. The UV spectra were obtained with a Hitachi U-4000 spectroscopy. Transmission electron microscopy was performed in Philip CM-200 TWIN TEM microscopy. The nanoparticle samples dissolved in toluene solution were drop cast onto a 200 mesh carbon-coated copper grid sample holder followed by natural evaporation at room temperature.

(20) Maye, M. M.; Zheng, W.; Leibowitz, F. L.; Ly, N. K.; Zhong, C. J. *Langmuir* **2000**, *16*, 490−497.

(21) Chidsey, C. E. D.; Loiacono, D. N. *Langmuir* **1990**, *6*, 682−691.

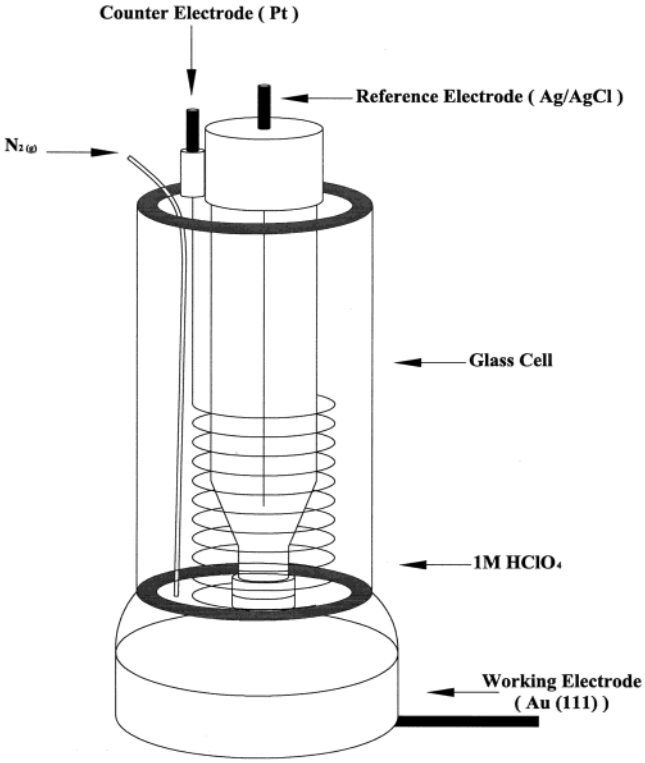

Figure 1. Schematic diagram of drop cell used for CV measurements on Au(111) electrodes.

Results and Discussion

In the following sections, we first present the characterization data of MPCs using TEM, UV−vis, and NMR techniques. We then present the electrochemical measurements of SAMs and MPCs.

Characterizations of MPCs 5a−c. The biferrocenate MPCs were characterized by a number of techniques: TEM for particle size and shape, UV−vis for particle size, and NMR for adsorption of biferrocenyl thiols.

TEM Imaging. Our TEM data of biferrocenethiolate MPCs showed an average core size of 4.4 ± 0.2 nm in the cases of **5a** and **5b**. For **5c**, an average core size of 5.0 ± 0.2 nm was observed. A representative TEM micrograph of **5c** is shown in Figure 2. The particle sizes appear uniform with a narrow distribution. A close examination of the particle shape reveals that some percentage of particles seem to exhibit "hexagon" outlines.

UV−Vis Measurement. Optically, both intensity and energy of the surface plasmon (SP) resonance bands of nanoparticles are known to be strongly dependent on size.[17,22,23] Figure 3 shows a set of UV−vis spectra of **5a−c**. The spectrum for the 4.5 nm octanethiolate MPCs shows identifiable SP band at 515 nm. The shape and position of this band are in agreement with those previously reported.[11] Spectra of biferrocenethiolate MPCs exhibited a significant change in the intensity for the SP band at 520 nm (**5a−c**). The feature of the SP band is in agreement with those obtained for 4−6 nm Au nanoparticles. The increased intensity of the SP band, without an apparent shift in energy, is indicative of an increase in core size.

NMR Spectroscopic Analysis. The NMR technique is used to confirm an important question which is whether

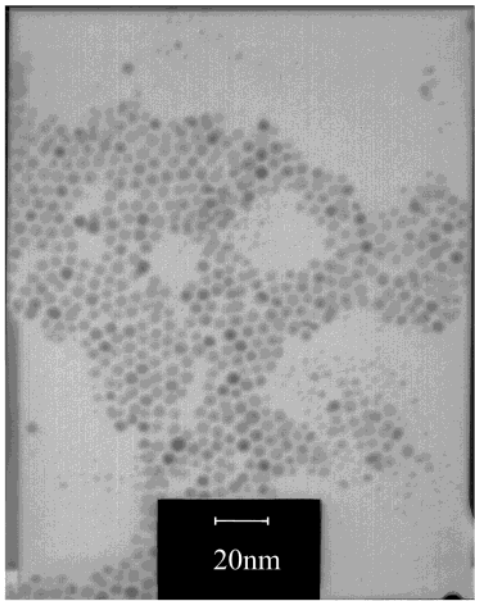

Figure 2. TEM micrograph of **5c**.

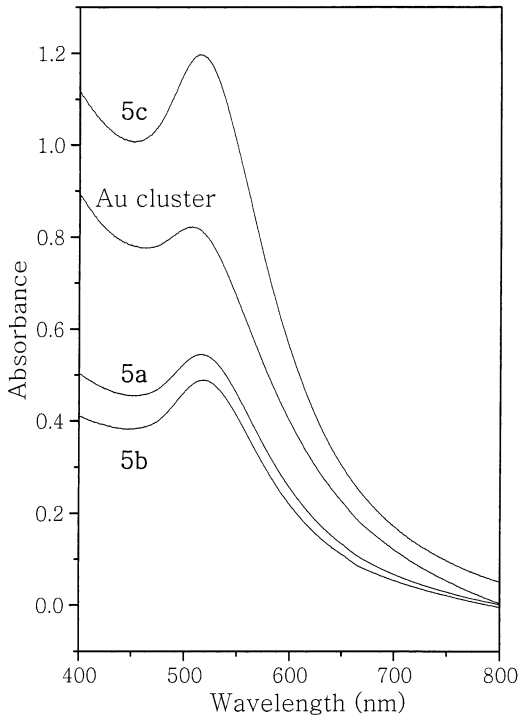

Figure 3. UV−vis spectra of **5a−c**. The samples (1 mg) are dissolved in CH_2Cl_2 (10 mL) solution.

the organic shell is functionalized by biferrocenyl alkanethiol. Figure 4 shows the representative ^{13}C NMR spectra for the octanethiolate Au nanoparticle (a) and the biferrocenyl alkanethiolate nanoparticles (b−d). The high field (10−40 ppm) broad peaks in Figure 4a establish the resonances as coming from the $-CH_{2-}$ and $-CH_3$ groups in octanethiol. The observation of broad feature results from the effects of paramagnetic relaxation. As shown in Figure 4b−d, the confirmation of the functionalization of biferrocenyl alkanethiol comes from the low field peaks (65−70 ppm), which are established the resonances of Cp moieties. Furthermore, the resonances of the $-CH_{2-}$ and $-CH_3$ groups in biferrocenylalkanethiol are also occurred in the range of 10 and 40 ppm. An interesting finding is that the biferrocenyl alkanethiol gives sharper NMR signals at room temperature in comparison with oc-

(22) Fink, J.; Kiely, C. J.; Bethell, D.; Schiffrin, D. J. *Chem. Matt.* **1998**, *10*, 922−926.
(23) Alvarez, M. M.; Khoury, J. T.; Schaaff, T. G.; Shafigullin, M. N.; Vezmar, I.; Whetten, R. L. *J. Phys. Chem. B* **1997**, *101*, 3706−3712.

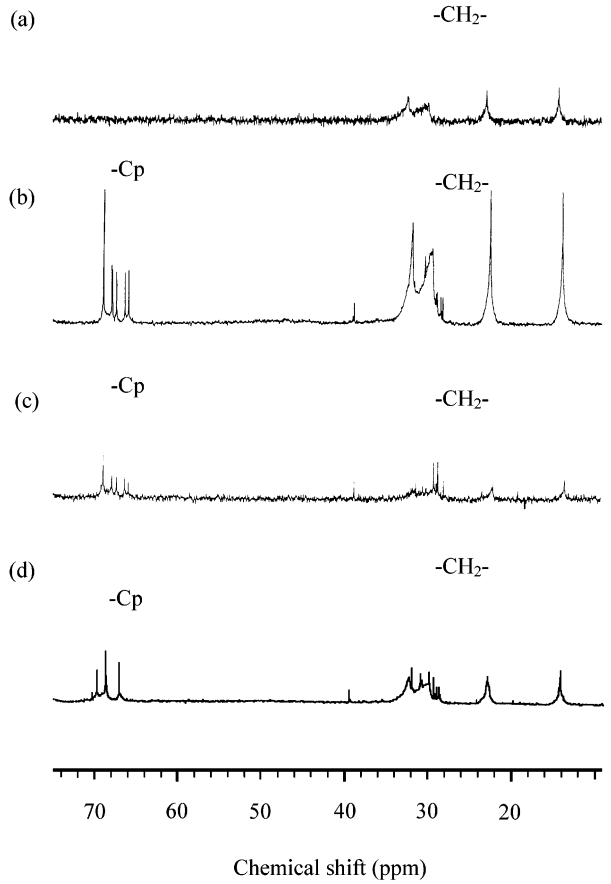

Figure 4. ^{13}C NMR spectra for the octanethiol Au nanoparticle (a), **5a** (b), **5b** (c), and **5c** (d) in $CDCl_3$ solution.

tanethiolate MCPs. We would like to suggest that the faster electron relaxation caused by the Fe centers decreases the efficiency of the nuclear relaxation mechanism, lengthening T_1 for the nucleus and causing the line to sharper.

Electrochemical Measurements of Free Ligands 1a−c. One of the interesting attributes of **1a−c** is the magnitude of the interaction between the two Fe sites. Cyclic voltammetry affords a simple and effective way for estimating this interaction.[24] Electrochemical data of the free thiols are given in Table 1. The CV studies show two successive one-electron redox waves that correspond to the redox behavior of the biferrocenyl moiety. As shown in Table 1, the first half-wave potentials of **1a−c** (0.34, 0.33, and 0.33 V, respectively) are less than that of biferrocene (0.37 V). From the electron-donating effect of the alkyl substituent, we believe that the first oxidation in **1a** and **1b** occurs at the alkyl ferrocenyl moiety. In the cases of **1c**, it is difficult to predict which ferrocenyl moiety is oxidized first from the electrochemical data.

It has been demonstrated that the magnitude of $\Delta E_{1/2}$ gives an indication of the interaction between the two Fe sites. In the case of symmetric biferrocene, it is the larger $\Delta E_{1/2}$ value the stronger Fe−Fe interaction.[24] For asymmetric biferrocene, the zero-point energy difference between two vibronic states also plays an important role in determining the magnitude of $\Delta E_{1/2}$ value. In the cases of **1a** and **1b**, the zero-point energy difference leads to a larger $\Delta E_{1/2}$ value in comparison with **1c** and biferrocene. For **1c**, the zero-point energy difference is rather small, which is reasonable in terms of the similar electronic effect between the pentyl substituent and pentyl thiol substituent. Therefore, the magnitude of the electronic interaction between the two Fe sites in **1c** is larger than that of biferrocene.

Table 1. Cyclic Voltammogram Data of Free Thiols 1a−c in CH_2Cl_2/CH_3CN (1:1)

compd	$E_{1/2}$ (V)[a]	$\Delta E_{1/2}$ (V)[b]	ΔE_p (mV)[c]	$10^{-5}K_{com}$[d]
1a	0.34	0.37	65	18.67
	0.71		65	
1b	0.33	0.38	92	27.59
	0.71		77	
1c	0.33	0.35	68	8.55
	0.68		61	
Bifc	0.37	0.31	70	1.78
	0.68		75	

[a] All half-wave potentials are referred to the Ag/AgCl electrode. Ferrocene shows a reversible one-electron oxidation wave at $E_{1/2}$ = 0.44 V in CH_2Cl_2/CH_3CN (1:1) solution. [b] Peak separation between two redox waves. [c] Peak to peak separation between the resolved reduction and oxidation waves maxima. [d] Comproportionation equilibrium constant.

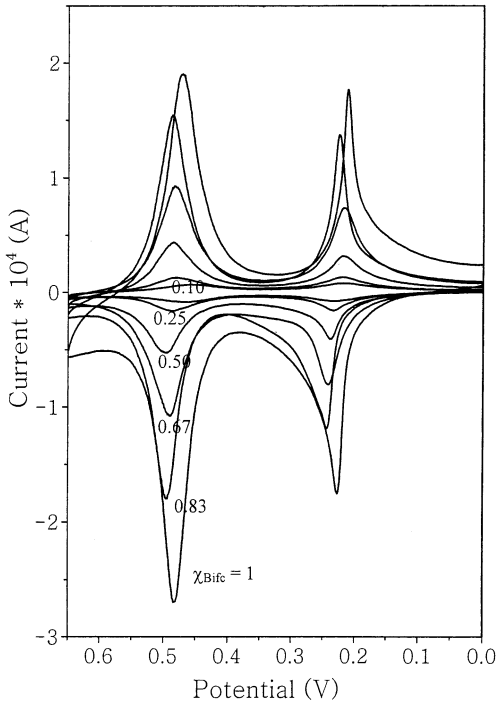

Figure 5. Cyclic voltammograms in 1 M $HClO_4$ of mixed monolayers of **4a** and 1-pentanethiol formed from ethanol solutions containing various mole fractions (χ_{Bifc}) of **4a**. Scan rate = 100 mVs^{-1}.

Electrochemical Measurements of SAMs 4a−c. As expected, the redox behavior of SAMs **4a−c** is dominated by the ferrocene/ferrocenium couples. The stability, surface charge coverage, and electron-transfer mechanism were assessed by cyclic voltammetry. Figures 5−7 show cyclic voltammograms of Au(111) electrodes modified by biferrocenyl alkanethiols (**1a−c**) in 1M $HClO_4$ solution. The electrochemical parameters obtained from the CV (Γ, surface coverage; $E_{1/2}$, half-wave potential; ΔE_p, redox peak separation) are summarized in Table 2. Repeat scanning does not change the voltammograms, demonstrating that these monolayers are stable to electrochemical cycling in acidic aqueous $HClO_4$ solution.

(24) (a) Atzkern, H.; Huber, B.; Köhler, F. H.; Müller, G.; Müller, R. *Organometallics* **1991**, *10*, 238−244. (b) Bunel, E. E.; Campos, P.; Ruz, P.; Valle, L.; Chadwick, I.; Ana, M. S.; Gonzalez, G.; Manriquez, J. M. *Organometallics* **1988**, *7*, 474−476. (c) Cowan, D. O.; Shu, P.; Hedberg, F. L.; Rossi, M.; Kistenmacher, T. J. *J. Am. Chem. Soc.* **1979**, *101*, 1304−1305. (d) Moulton, R.; Weidman, T. W.; Vollhardt, K. P. C.; Bard, A. J. *Inorg. Chem.* **1986**, *25*, 1846−1851. (e) Obendorf, D.; Schottenberger, H.; Rieker, C. *Organometallics* **1991**, *10*, 1293−1297.

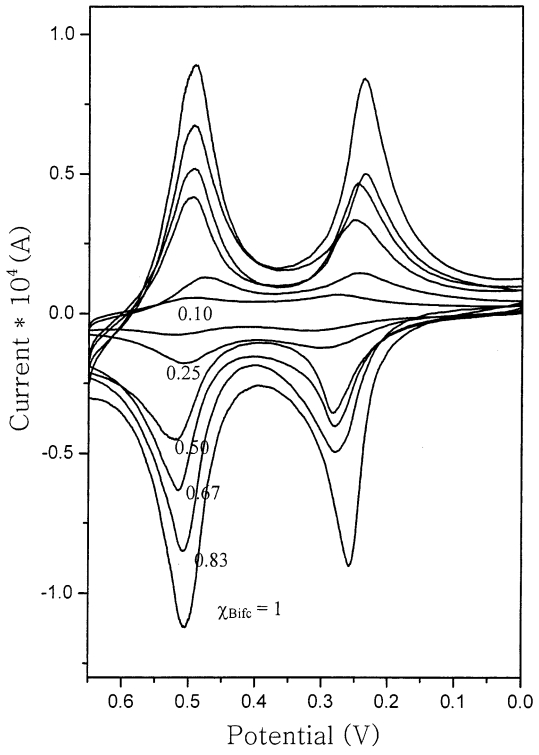

Figure 6. Cyclic voltammograms in 1 M $HClO_4$ of mixed monolayers of **4b** and 1-octanethiol formed from ethanol solutions containing various mole fractions (χ_{Bifc}) of **4b**. Scan rate = 100 mVs^{-1}.

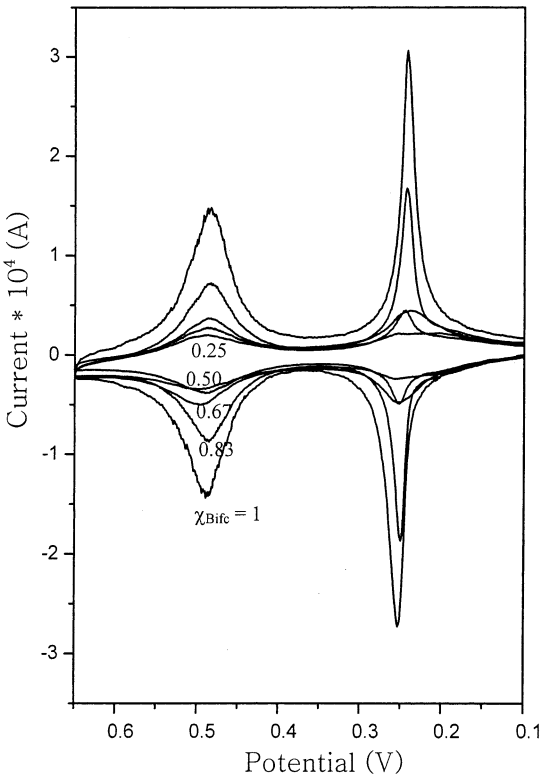

Figure 7. Cyclic voltammograms in 1 M $HClO_4$ of mixed monolayers of **4c** and 1-pentanethiol formed from ethanol solutions containing various mole fractions (χ_{Bifc}) of **4c**. Scan rate = 100 mVs^{-1}.

As given in Table 2, the values of $\Delta E_{1/2}$ (~0.25 V) are smaller in comparison with those of free biferrocenyl alkanethiols (~0.37 V). The factors that are potentially important in controlling the interaction between the two

Table 2. Electrochemical Data Extracted from the CV with Scan Rate of 100 mVs^{-1}

SAMs	χ_{Bifc}	$E_{1/2}$ (V)[a]	$\Delta E_{1/2}$ (V)[a]	ΔE_p (mV)	Γ[b]	peak width (mV)[c]
4a	1	0.22	0.26	24	2.05	24, 53
		0.48		15		39, 45
	0.83	0.23	0.26	24	1.71	24, 29
		0.49		9		47, 41
	0.67	0.23	0.26	19	1.42	46, 58
		0.49		6		39, 55
	0.50	0.23	0.26	16	0.94	48, 58
		0.49		9		38, 57
	0.25	0.23	0.25	10	0.42	66, 73
		0.48		1		46, 67
	0.10	0.22	0.24	14	0.25	80, 79
		0.46		10		73, 80
4b	1	0.25	0.25	27	2.65	67, 60
		0.50		10		64, 54
	0.83	0.26	0.24	44	1.92	63, 65
		0.50		13		76, 63
	0.67	0.26	0.25	33	1.42	71, 67
		0.51		16		57, 68
	0.50	0.27	0.24	28	0.97	80, 66
		0.51		10		52, 79
	0.25	0.27	0.22	30	0.54	87, 65
		0.49		8		98, 77
	0.10	0.29	0.22	33	0.15	81, 72
		0.51		6		97, 86
4c	1	0.25	0.24	8	3.27	16, 47
		0.49		1		22, 49
	0.83	0.25	0.24	7	2.09	17, 51
		0.49		2		16, 54
	0.67	0.25	0.24	7	1.87	28, 61
		0.49		3		26, 72
	0.50	0.25	0.24	10	1.24	53, 56
		0.49		8		45, 62
	0.25	0.25	0.24	7	0.92	95, 70
		0.49		7		77, 79

[a] The first redox wave is listed first. [b] In unit of $\times 10^{14}$ molecule cm^{-2}. [c] The total width at half-height with scan rate of 100 mVs^{-1}. The width of the cathodic wave is listed first.

Fe centers in a biferrocenium cation include (1) the electronic coupling and the zero-point energy difference between the two Fe centers, (2) the reorganization energy of solvent, and (3) the reorganization energy of the cation. The electrochemical measurements for free biferrocenyl alkanethiols and SAMs (**4a**−**c**) are carried out in the solutions of CH_2Cl_2/CH_3CN (1:1) and 1M aqueous $HClO_4$, respectively. The linear direct proportion of Fe−Fe interaction with solvent dielectric properties has been observed for several mixed-valence compounds.[25] The magnitude of the electronic coupling and zero-point energy difference between the two vibronic states of the biferrocenyl moirty in SAMs are similar with those of corresponding free biferrocenyl alkanethiol, which is reasonable in terms of the similar structural geometry of the biferrocenyl moiety. Therefore, we would suggest that the magnitude of the reorganization energy of cation leads to smaller $\Delta E_{1/2}$ values in the case of SAMs. For an iron metallocne, the distance between Fe and Cp ring centroid changes from 1.65 Å for Fe(II) to 1.70 Å for Fe(III).[26,27] When an intramolecular electron transfer occurs in a biferrocenium cation, the two Cp rings bound to the Fe(II) ion move away from the metal to adjust their distance to the larger dimension appropriate for an $Fe^{III}(Cp)_2$ moiety.

(25) (a) Tom, G. M.; Creutz, C.; Taube, H. *J. Am. Chem. Soc.* **1974**, *96*, 7827−7829. (b) Powers, M. J.; Meyer, T. J. *J. Am. Chem. Soc.* **1978**, *100*, 4393−4398. (c) Powers, M. J.; Callahan, R. W.; Salmon, D. J.; Meyer, T. J. *Inorg. Chem.* **1976**, *15*, 1457−1459.

(26) Seiler, P.; Dunitz, J. D. *Acta Crystallogr., Sect. B* **1979**, *35*, 1068−1074.

(27) Mammano, N. J.; Zalkin, A.; Landers, A.; Rheingold, A. L. *Inorg. Chem.* **1977**, *16*, 297−300.

Table 3. Standard Electron Transfer Rate Constant[a]

scan rate (mVs^{-1})		100		200		300		400		500	
SAMs	χ_{Bifc}	ΔE_p	k_s	ΔE_p	k_s	ΔE_p	k_s	ΔE_p	k_s	ΔE_p	k_s
4a	1	24	6.1	40	6.7	48	8.1	50	10.4	55	11.6
		15	11.1	22	13.6	33	12.6	36	15.1	37	18.3
	0.83	24	6.1	31	9.0	36	11.3	41	13.0	45	14.6
		9		12	30.6	17	28.3	19	32.6	23	32.2
	0.67	19	8.2	27	10.6	35	11.7	40	13.4	46	14.2
		6		8		10		11	69.8	15	55.7
	0.5	16	10.2	22	13.6	28	15.2	33	16.7	42	15.8
		9		14	24.5	18	26.2	24	24.4	31	22.5
	0.25	10		14	24.5	21	21.6	22	27.2	25	29.0
		1		4		7		8		9	
4b	1	27	5.3	35	7.8	44	9.0	53	9.7	57	11.1
		10		16	20.4	18	26.2	22	27.2	26	27.7
	0.83	44	3.0	53	4.8	58	6.6	48	10.9	50	13.0
		13	13.6	18	17.5	22	20.4	26	22.2	29	24.3
	0.67	33	4.182	34	8.079	42	9.492	49	10.60	56	11.37
		16	10.2	18	17.5	24	18.3	26	22.2	30	23.4
	0.5	28	5.1	34	8.1	39	10.3	41	13.0	48	13.6
		10		13	27.2	18	26.2	25	23.2	29	24.3
	0.25	30	4.7	59	4.3	69	5.4	78	6.2	90	6.5
		8		12	30.6	16	30.6	20	30.6	24	30.5
4c	1	8		12	30.6	15	33.4	19	32.6	20	38.2
		1		3		4		6		6	
	0.83	7		10		14	36.7	15	44.5	17	47.1
		2		1		5		5		6	
	0.67	7		10		13	40.8	16	40.8	20	38.2
		3		3		3		6		5	
	0.5	10		11	34.9	15	33.4	17	37.7	20	38.2
		8		8		11	52.4	13	54.4	15	55.7
	0.25	7		7		6		8		11	87.29
		7		4		4		4		9	

[a] The k_s value is conveniently determined by monitoring the peak separation (ΔE_p), using Laviron's formalism and assuming an α value close to 0.5. Due to experimental error caused by the convergence of the anodic and cathodic peak potentials, the rate is calculated with $\Delta E_p > 10$ mV. The first redox wave is listed first.

At the same time, the dimensions of the $Fe^{III}(Cp)_2$ moiety contract to those of an $Fe^{II}(Cp)_2$ species. In the case of free biferrocenyl alkanethiols in CH_2Cl_2/CH_3CN solution, the cation is solvated, and it can move rapidly so as not to limit the rate of intramolecular electron transfer. For immobile electroactive groups of SAMs, the two Cp rings bound to the Fe center cannot rapidly adjust their dimensions when electron transfer occurs. Consequentially, it leads to smaller $\Delta E_{1/2}$ values.

As described in the section of introduction, broadened electrochemical features were observed for electrodes modified with ferrocenyl alkanethiols ($Fc(CH_2)_nSH$) and $BifcCO(CH_2)_nSH$ derivatives.[4,13−16] Interestingly, this is not what we observed. For **4a**−**c**, the biferrocene redox waves are symmetric and with small splitting between the oxidation and reduction peaks. Furthermore, the peak current is proportional to the scan rate (ν), in contrast to the $\nu^{1/2}$ dependence observed for Nernstian waves of diffusing species. Using unsubstituted alkanethiol as coadsorbates results in very similar cyclic voltammograms for $\chi_{Bifc} = 0.10$, 0.25, 0.50, 0.67, 0.83, and 1.00. For an ideal Nernstian reaction under $E_{pa} = E_{pc}$ (E_{pa}, anodic peak potential; E_{pc}, cathodic peak potential), the total width at half-height of either the cathodic or anodic wave is estimated as 90 mV at 25 °C.[28] The peak current is also proportional to the scan rate, and the total width at half-height of either the cathodic or anodic wave with the scan rate of 100 mVs^{-1} for the various mole fraction of electroactive groups is given in Table 2. The values of the total width at half-height for the various χ_{Bifc} are smaller, 90 mV. This result is possible due to the electron hopping (intramolecular electron transfer) between the two Fe centers, and the intermolecular interaction between the biferrocenyl moieties. The deviation from the expected value of 90 mV is more significant in the case of **4c**. In comparison with **4a** and **4b**, the zero-point energy difference between the two vibronic states of the biferrocenyl moieties is almost equal to zero. This is reasonable in terms of the similar electronic effects of $-(CH_2)_4CH_3$ and $-(CH_2)_5SH$ substituents. Consequently, the intramolecular electron-transfer rate between the two Fe centers in **4c** is faster than that of **4a** and **4b**. The electron hopping mechanism in **4c** would play a more important role in determining the magnitude of peak width.

As given in Table 2, the splitting between the oxidation and reduction peaks corresponds to a standard electron-transfer rate constant (k_s).[29−31] The k_s value is conveniently determined by monitoring the peak separation of the CV wave as a function of sweep rate.[29] These results are given in Table 3, assuming an α value close to 0.5. The data at higher mole fraction calculated using Laviron's formalism are not well constant, primarily due to a convergence of the anodic and cathodic peak potentials at slow sweep rates and intermolecular interaction between the biferrocenyl moieties. This phenomenon was observed more significantly at higher mole fraction of electroactive groups. The data in Table 3 do not suggest the presence of ohmic errors, since a systematic decrease values of k_s at higher sweep rates is not found. At lower mole fraction ($\chi_{Bifc} < 0.5$), the k_s calculated are well constant. Ohmic

(28) Murray, R. W. In *Electroanalytical Chemical*; Bard, A. J., Ed., Marcel Dekker: New York, 1984; Vol. 13, pp 191−368.

(29) Standard rate constants are calculated as recommended by Laviron assuming $\alpha = 1/2$.

(30) Laviron, E. *J. Electroanal. Chem.* **1979**, *101*, 19−28.

(31) (a) Creager, S.; Yu, C. J.; Bamdad, C.; O'Conner, S.; MacLean, T.; Lam, E.; Chong, Y.; Olsen, G. T.; Luo, J.; Gozin, M.; Kayyem, J. F. *J. Am. Chem. Soc.* **1999**, *121*, 1059−1064. (b) Weber, K.; Hockett, L.; Creager, S. *J. Phys. Chem. B* **1997**, *101*, 8286−8291.

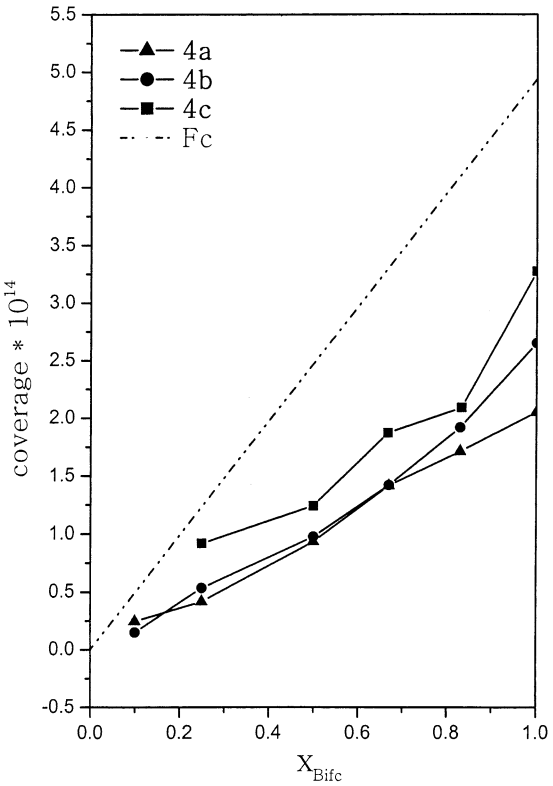

Figure 8. Biferrocene surface coverage for mixed monolayers of **4a** (▲), **4b** (●), and **4c** (■) as a function of the mole fraction (χ_{Bifc}) of the biferrocene alkanethiol in the adsorption solution. Dotted line is ferrocene coverage calculated for a close-packed model.

error is not obvious in these data. The minimum ohmic error occurs at the lowest sweep rate, for which the current is minimum. The peak current in the voltammogram at the highest sweep rate approximately 250 μA in the case of $\chi_{Bifc} = 0.5$. Ohmic losses are small enough at lower mole fraction of electroactive groups that they may be ignored. An interesting finding is that the standard rate constant of the second redox wave is always greater than that of the first redox wave. Theoretically, we expect that the interaction between the two Fe centers leads to a larger standard rate constant for the second redox wave. In the existence of the stronger Fe−Fe interaction, the oxidation potential of the second wave shifts to the higher voltage and the reduction potential of the second wave shifts to the lower voltage, when the charge density of the biferrocenyl moiety caused by the oxidization of one of the ferrocenyl moieties increases. In other words, the intramolecular electron hopping mechanism may play an important role in determining the magnitude of k_s value.

The amount of electroactive biferrocene in the monolayers can be calculated from the cyclic voltammograms shown in Figures 5 and 6. The area under the peaks is integrated and divided by the scan rate to obtain the amount of charge passed to oxidize the biferrocene or reduce the biferrocenium sites. The surface charge densities (μC/cm^2) obtained by this procedure are converted to biferrocene surface coverages by dividing by the electron charge. Figure 8 shows biferrocene surface coverages plotted versus the mole fraction of biferrocenyl alknaethiol of **4a**−**c**. The surface coverages of electroactive biferrocenyl alkanethiols are smaller than the maximum theoretical value (dotted line in Figure 8, 4.94×10^{14} molecule cm^{-2} at $\chi_{Fc} = 1$) calculated for a close-packed monolayer of ferrocene derivatives.[4] As shown in Figure 8, electrodes modified by immersion in more concentrated solutions

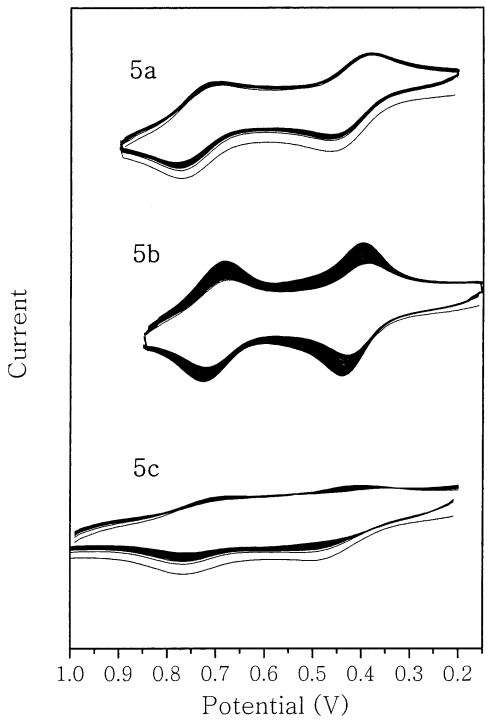

Figure 9. Cyclic voltammograms of **5a**−**c** for consecutive potential scans at 100 mVs^{-1}.

exhibit higher coverages. The amount of compound deposited on the gold surface depends on the concentration of the deposition solution and temperature; however, the influence of the latter was not systematically investigated in this work. Hence, the modified electrodes reported here were formed at room temperature. Figure 8 also shows that increasing the length of the polymethylene chains from **4a** to **4b** does not drastically effect to biferrocene coverage at low mole fraction ($\chi_{Bifc} \leq 0.67$). This trend is similar to effects seen in mixed monolayer systems of $FcCO_2(CH_2)_{11}SH$ and $FcCO_2(CH_2)_{16}SH$.[4] However, at constant mole fraction of biferrocenyl alkanethiol in the adsorption solution, the biferrocene coverage in **4c** is always the largest than those of **4a** and **4b**. This can, at least in part, be explained by the relative solubilities of the coadsorbates in the ethanol adsorption solutions. If alkanethiol is less soluble in ethanol, its free energy in solution will be higher and its affinity for adsorption should be larger.

Electrochemical Measurements of MPCs 5a−c. Cyclic voltammograms of **5a**−**c** for consecutive potential scans are shown in Figure 9. The electrochemical parameters are summarized in Table 3. As expected, two reversible redox waves were observed, the peak current is roughly proportional to the potential scan rate, and the wave shape is roughly symmetrical. The peak-to-peak separation is small (68−40 mV for **5a** and **5c**; 28 mV for **5b**). These factors are all consistent with most of current arising from reaction of an adsorbed layer of ferrocenated MPCs.[13−15]

The values of $\Delta E_{1/2}$ are intermediate between the analogues values for free biferrocenyl alkanethiols and biferrocenate SAMs. This is a reflection of the magnitude of reorganization energy of cation. The values of ΔE_p are larger in comparison with the analogues values of biferrocenated SAMs. The increase in ΔE_p can be attributed to kinetic effects, but the detailed studies requires for a certain assignment have not been carried out. The standard rate constant of electron transfer was calculated from the value of ΔE_p with the scan rate of 100 mVs^{-1} and

Table 4. Electrochemical Data Extracted from the CV with Scan Rate of 100 mV s^{-1}

MPCs	$E_{1/2}$ (V)[a]	$\Delta E_{1/2}$ (V)[a]	ΔE_p (mV)	k_s (s^{-1})[b]	
5a	0.42, 0.74	0.32	68, 63	1.7	1.8
5b	0.42, 0.70	0.28	41, 37	3.1	3.6
5c	0.45, 0.72	0.27	58, 50	2.1	2.5

[a] The first redox wave is listed first. [b] Standard rate constant of electron transfer. The calculated rate for the first redox wave is listed first.

given in Table 3. A similar observation with SAMs was also found that the standard rate constant of the second redox wave is larger than that of the first redox wave. In the case of Bifc−$CO(CH_2)_7S$− carbonyl-functionalized MPC reported by Nishihara,[13−15] broadened redox waves were observed with the scan number increased in a potential range between −0.3 and 0.9 V versus Ag/Ag^+. Nishihara suggested that this is an occurrence of electroactive film formation at the electrode. In our cases, this is not what we observed, indicating that noninteracting and homogeneous electroactive groups are attached to the cluster surface.

Acknowledgment. Our work was generous supported by the National Science Council (NSC92-2113-M-110-011), Taiwan, ROC, and Department of Chemistry and Center for Nanoscience and Nanotechnology at Sun Yat-Sen University.

LA0303714